Colorless directional coupler with dispersion engineered sub-wavelength structure

R. Halir,[1,*] A. Maese-Novo,[1] A. Ortega-Moñux,[1] I. Molina-Fernández,[1] J. G. Wangüemert-Pérez,[1] P. Cheben,[2] D.-X. Xu,[2] J. H. Schmid,[2] and S. Janz[2]

[1]*Departamento Ingeniería de Comunicaciones, ETSI Telecomunicación, Universidad de Málaga, 29010 Málaga, Spain*

[2]*Institute for Microstructural Sciences, National Research Council of Canada, Ottawa, Ontario, K1A 0R6, Canada*

[*]*robert.halir@ic.uma.es*

Abstract: Directional couplers are extensively used devices in integrated optics, but suffer from limited operational wavelength range. Here we use, for the first time, the dispersive properties of sub-wavelength gratings to achieve a fivefold enhancement in the operation bandwidth of a silicon-on-insulator directional coupler. This approach does not compromise the size or the phase response of the device. The sub-wavelength grating based directional coupler we propose covers a 100 nm bandwidth with an imbalance of ≤ 0.6 dB between its outputs, as supported by full 3D FDTD simulations.

OCIS codes: (130.3120) Integrated optics devices; (050.6624) Subwavelength structures; (260.2030) Dispersion; (230.7370) Waveguides.

References and links

1. S.-H. Hsu, "Optical waveguide tap with low polarization dependence and flattened wavelength using a Mach–Zehnder directional coupler," Appl. Opt. **49**, 2434–2440 (2010).
2. T. Lee, D. Lee, and Y. Chung, "Design and simulation of fabrication-error-tolerant triplexer based on cascaded Mach–Zehnder inteferometers," IEEE Photon. Technol. Lett. **20**, 33–35 (2008).
3. D. M. Beggs, T. P. White, L. O'Faolain, and T. F. Krauss, "Ultracompact and low-power optical switch based on silicon photonic crystals," Opt. Lett. **33**, 147–149 (2008).
4. D.-X. Xu, M. Vachon, A. Densmore, R. Ma, A. Delâge, S. Janz, J. Lapointe, Y. Li, G. Lopinski, D. Zhang, Q. Y. Liu, P. Cheben, and J. H. Schmid, "Label-free biosensor array based on silicon-on-insulator ring resonators addressed using a WDM approach," Opt. Lett. **35**, 2771–2773 (2010).
5. L. Soldano and E. Pennings, "Optical multi-mode interference devices based on self-imaging: principles and applications," J. Lightwave Technol. **13**, 615–627 (1995).
6. R. Halir, G. Roelkens, A. Ortega-Moñux, and J. G. Wangüemert-Pérez, "High-performance 90° hybrid based on a silicon-on-insulator multimode interference coupler," Opt. Lett. **36**, 178–180 (2011).
7. B. Little and T. Murphy, "Design rules for maximally flat wavelength-insensitive optical power dividers using Mach–Zehnder structures," IEEE Photon. Technol. Lett. **9**, 1607–1609 (1997).
8. Q. Wang and S. He, "Optimal design of planar wavelength circuits based on Mach–Zehnder interferometers and their cascaded forms," J. Lightwave Technol. **23**, 1284–1290 (2005).
9. J. Gamet, G. Pandraud, S. Opsitech, and F. Grenoble, "C-and L-band planar delay interferometer for DPSK decoders," IEEE Photon. Technol. Lett. **17**, 1217–1219 (2005).
10. Y. Shani, C. Henry, R. Kistler, R. Kazarinov, and K. Orlowsky, "Integrated optic adiabatic devices on silicon," IEEE J. Quantum Electron. **27**, 556–566 (1991).
11. G. Paloczi, A. Eyal, and A. Yariv, "Wavelength-insensitive nonadiabatic mode evolution couplers," IEEE Photon. Technol. Lett. **16**, 515 –517 (2004).

#164215 - $15.00 USD Received 6 Mar 2012; revised 26 Mar 2012; accepted 27 Mar 2012; published 31 May 2012

12. C. Doerr, M. Cappuzzo, E. Chen, A. Wong-Foy, L. Gomez, A. Griffin, and L. Buhl, "Bending of a planar lightwave circuit 2×2 coupler to desensitize it to wavelength, polarization, and fabrication changes," IEEE Photon. Technol. Lett. **17**, 1211–1213 (2005).
13. P. Cheben, D. Xu, S. Janz, and A. Densmore, "Subwavelength waveguide grating for mode conversion and light coupling in integrated optics," Opt. Express **14**, 4695–4702 (2006).
14. R. Halir, P. Cheben, J. H. Schmid, R. Ma, D. Bedard, S. Janz, D.-X. Xu, A. Densmore, J. Lapointe, and I. Molina-Fernández, "Continuously apodized fiber-to-chip surface grating coupler with refractive index engineered subwavelength structure," Opt. Lett. **35**, 3243–3245 (2010).
15. U. Levy, M. Abashin, K. Ikeda, A. Krishnamoorthy, J. Cunningham, and Y. Fainman, "Inhomogenous dielectric metamaterials with space-variant polarizability," Phys. Rev. Lett. **98**, 243901 (2007).
16. P. J. Bock, P. Cheben, J. H. Schmid, J. Lapointe, A. Delâge, D.-X. Xu, S. Janz, A. Densmore, and T. J. Hall, "Subwavelength grating crossings for silicon wire waveguides," Opt. Express **18**, 16146–16155 (2010).
17. P. Cheben, P. J. Bock, J. H. Schmid, J. Lapointe, S. Janz, D.-X. Xu, A. Densmore, A. Delâge, B. Lamontagne, and T. J. Hall, "Refractive index engineering with subwavelength gratings for efficient microphotonic couplers and planar waveguide multiplexers," Opt. Lett. **35**, 2526–2528 (2010).
18. A. Ortega-Monux, L. Zavargo-Peche, A. Maese-Novo, I. Molina-Fernandez, R. Halir, J. Wanguemert-Perez, P. Cheben, and J. Schmid, "High-performance multimode interference coupler in silicon waveguides with subwavelength structures," IEEE Photon. Technol. Lett. **23**, 1406–1408 (2011).
19. L. Zavargo-Peche, A. Ortega-Moñux, J. G. Wangüemert-Pérez, and I. Molina-Fernández, "Fourier based combined techniques to design novel sub-wavelength optical integrated devices," Prog. Electromagn. Res. **123**, 447–465 (2012).
20. M. Robertson, S. Ritchie, and P. Dayan, "Semiconductor waveguides: analysis of optical propagation in single rib structures and directional Couplers," IET Optoelectron. **132**, 336–342 (1985).

1. Introduction

Directional couplers are widely used devices in integrated optics, with applications including optical taps, wavelength demultiplexers, optical switches and biosensors [1–4]. Directional couplers are straightforward to design and their splitting ratio is readily adjusted by varying their length or waveguide separation. However, especially when compared to multi-mode interference (MMI) devices, their bandwidth is limited [5], which is why the latter are preferred for some applications [6].

Several methods have been proposed to enhance the bandwidth of directional couplers. By connecting couplers in a Mach-Zehnder interferometer their responses can be compensated [7–9], but at the cost of a considerably larger device. Adiabatic mode conversion couplers achieve broadband operation by using specific, tapered shapes in the coupling region, which, again, increase device size significantly [10, 11]. Finally, bending of the complete coupler enhances its bandwidth, but results in degradation of its phase response [12].

Here we propose, for the first time, the use of sub-wavelength gratings (SWGs) to design broadband directional couplers. SWGs, in which diffraction is suppressed by using a sub-wavelength pitch, have been used successfully to synthesize previously unavailable refractive indices in fibre-to-chip couplers [13, 14], metamaterial lenses [15], waveguide crossings [16], multiplexers [17], and multi-mode interference couplers [18]. However, the dispersive properties of SWGs remain, to the best of our knowledge, unexplored. In this paper, we show that using these properties a fivefold gain in bandwidth can be achieved for a directional coupler in silicon. As opposed to previous approaches [7–12], our design yields devices with virtually the same length as conventional couplers and its impact on the phase response is marginal.

This paper is organized as follows. In section 2 we describe the general concept of how directional coupler bandwidth is increased using SWGs. The design of the device is detailed in section 3, where we also discuss the performance that is achieved. While we focus on a 50/50 splitter here, other splitting ratios can be obtained by simply changing the length of the coupler. Finally, in section 4 conclusions are drawn.

#164215 - $15.00 USD Received 6 Mar 2012; revised 26 Mar 2012; accepted 27 Mar 2012; published 31 May 2012

2. Concept

2.1. Conventional directional coupler

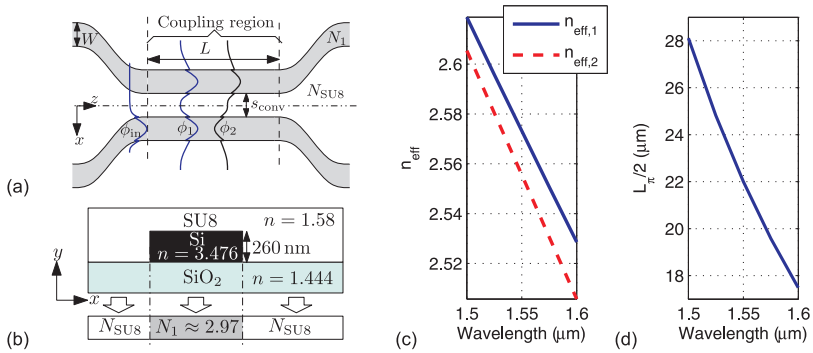

Fig. 1. (a) Schematic illustration of a conventional directional coupler. (b) Cross-sectional waveguide dimensions and effective index model. Refractive indices are given at $\lambda = 1.55\,\mu$m. (c) Effective indices and (d) half beat length of the even and odd supermodes, ϕ_1 and ϕ_2, of a conventional directional coupler as a function of wavelength.

The operation of a conventional directional coupler is illustrated in Fig. 1(a). Light is launched into one arm of the device, and excites the even and odd supermodes (ϕ_1 and ϕ_2) of the two parallel waveguides, which are separated a distance s_{conv}. The beat length of these modes is given by $L_\pi = \frac{\lambda/2}{n_{\text{eff},1} - n_{\text{eff},2}}$, where $n_{\text{eff},1}$ and $n_{\text{eff},2}$ are the effective indices of ϕ_1 and ϕ_2, respectively. By setting the physical length of the coupling region to $L = L_\pi/2$ a $50/50$ coupler is obtained. However, power splitting is perfectly symmetric only at the design wavelength, because L_π varies with wavelength due to modal dispersion. Intuitively this dependence can be understood as follows: as wavelength decreases, the even and odd modes become more confined inside the waveguides, so that $n_{\text{eff},1}$ and $n_{\text{eff},2}$ both tend towards the effective index of the isolated waveguides, thus increasing L_π. To exemplify this, consider a directional coupler based on the silicon wire waveguide shown in Fig. 1(b). The effective indices of the even and odd supermodes, $n_{\text{eff},1}$ and $n_{\text{eff},1}$, of such a coupler, with $W = 0.45\,\mu$m wide silicon wire waveguides separated by $s_{\text{conv}} = 0.3\,\mu$m, are plotted in Fig. 1(c) for the TE polarization. They converge as wavelength is decreased, resulting in an almost linear increase of L_π, as seen in Fig. 1(d). In this particular example $L_\pi/2$ exhibits a variation of about 20% between $\lambda = 1.5\,\mu$m and $\lambda = 1.6\,\mu$m. Even if the gap is reduced to $s_{\text{conv}} = 0.1\,\mu$m the variation is still about 13%.

2.2. Dispersion engineered directional coupler

We propose the directional coupler shown in Fig. 2(a), where the coupling section of the device is embedded in a subwavelength grating. By properly designing the pitch (Λ) and gap (g) of the SWG, the beat length of this structure becomes almost wavelength independent, enabling broadband operation. The operation principle is explained in the following. The pitch of the SWG (Λ) is small enough to ensure that diffraction is suppressed, so that at a fixed wavelength and angle of incidence it acts as a homogenous medium [17]. However, since the SWG used here is arrayed along the propagation direction z, the effective index of its fundamental Floquet mode will increase appreciably with wavelength as the Bragg wavelength, $\lambda_B = 2\Lambda n_{\text{eff}}$, is approached. This is illustrated in Fig. 2(b), where the effective index, n_{eff}, of the fundamental Floquet mode propagating through the structure shown in the inset is seen to increase rapidly as the Bragg wavelength, $\lambda_B \sim 1.48\,\mu$m, is approached.

#164215 - $15.00 USD Received 6 Mar 2012; revised 26 Mar 2012; accepted 27 Mar 2012; published 31 May 2012

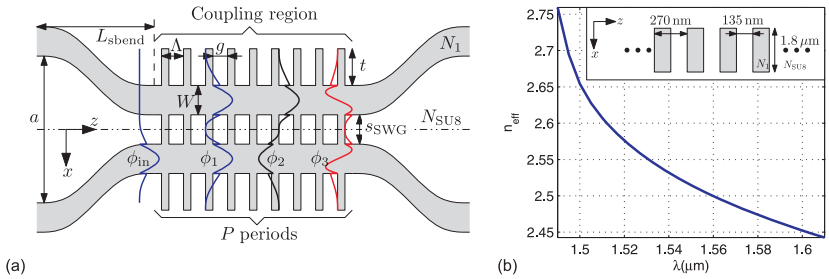

Fig. 2. (a) Schematic of the proposed broadband directional coupler. (b) Effective index of the fundamental Floquet mode propagating through the sub-wavelength grating shown in the inset.

Inserting the SWG between the coupler waveguides will have different effects on the effective indices $n_{\text{eff},1}$ and $n_{\text{eff},2}$ of the coupler's even and the odd supermodes, ϕ_1 and ϕ_2. Since the field of the odd supermode, ϕ_2, is asymmetric in central SWG region (between the waveguides), most of its index perturbation will cancel. Conversely, the effective index of the even mode, ϕ_1, which has a symmetric field in the central SWG, will change appreciably as the index of the SWG changes. As wavelength is decreased, both propagation constants are now affected by two opposing mechanisms: a) increased confinement tends to equate the effective indices, increasing L_π, and b) the SWG increases mainly $n_{\text{eff},1}$, so that L_π decreases. By properly adjusting the SWG variation of L_π with wavelength can be markedly reduced, enabling broadband operation.

3. Simulation and design

For our design we consider the silicon wire waveguide cross-section shown in Fig. 1(b) and TE (in-plane) polarized light, corresponding to TM in the 2D model. The concept is presented here for TE-like polarization, which is typically used in silicon microphotonic waveguides. However, it can be extended to TM (out-of-plane) polarized light, but, due to birefringence of the SWG, will generally result in different optimum device dimensions. The waveguide core consists of a 260 nm thick silicon layer that sits on a silicon dioxide layer, and is covered by SU-8 polymer. Simulations are based on the effective index model shown in Fig. 1(b), and carried out with an in-house, Fourier expansion based simulation tool [19] that takes into account material dispersion. This tools allows for the efficient calculation of the Floquet modes that govern the operation of the SWG based directional coupler. The final design is verified with full 3D FDTD simulations. Due to the sub-wavelength nature of the periodic structure in the coupling region the field profiles of the Floquet modes resemble the fields of modes in a homogenous waveguides. Consequently we will plot the Floquet mode field distributions only for a fixed value of z, in the center of a SWG air gap.

The design of the SWG based directional coupler encompasses three distinct steps. The first step is mainly related to the third order supermode, ϕ_3 in Fig. 2(a), which interferes with the operation of the coupler and must thus not be excited. In a second step the SWG structure is optimized to flatten the wavelength dependence of the beat length of the two first order supermodes (ϕ_1 and ϕ_2) with respect to wavelength. Finally, the complete structure shown in Fig. 2(a) is simulated and the optimum number of periods of the SWG (P), i.e. the coupling length, is determined.

#164215 - $15.00 USD Received 6 Mar 2012; revised 26 Mar 2012; accepted 27 Mar 2012; published 31 May 2012

3.1. Coupler excitation

In conventional directional couplers a sizeable amount of coupling can take place in the input and output s-bends of the device [Fig. 1(a)], apart from the central straight coupling section. In the design proposed here coupling in the s-bend regions has to be avoided, since the required wavelength independent coupling, i.e. constant L_π, is difficult to ensure when the separation between waveguides varies continuously. This is why a waveguide separation of $s_{\mathrm{SWG}} = 0.5\mu\mathrm{m}$ is adopted, which ensures that the access s-bends remain virtually decoupled.

In the SWG based coupler a third order supermode, ϕ_3, shown schematically in Fig. 2(a), is present. We have verified with 3D full vectorial simulations that this mode is also present in the conventional coupler, where it is weakly guided in the gap between the waveguides and virtually no power couples into it. This mode may be interpreted as the supermode resulting from the superposition of the second order modes of the individual waveguides. These are close to cut-off in the individual waveguides, but become guided as the waveguide separation is reduced. A detailed examination of this phenomenon is, however, out of the scope of this paper. In the SWG coupler a significant amount of power can couple into this third order mode. If ϕ_3 is excited it interferes with the operation of the directional coupler producing spurious power transfer between the waveguides.

The power coupled into this mode can however be controlled by adjusting the duty-cycle of the SWG, which we define as $\mathrm{DC} = (\Lambda - g)/\Lambda$, and the extent of the SWG on both sides of the coupler waveguides, t [see Fig. 2(a)]. We found that t should be $t \geq 400\,\mathrm{nm}$, so that modes see a symmetric refractive index distribution on both sides of the waveguides. This is important because, as discussed in the following, the amount of power that couples into ϕ_3 essentially depends on its anti-symmetry with respect to the waveguide center. Figure 3(a) shows the overlap of the third order supermode, ϕ_3, with the mode of the lower input waveguide, ϕ_{in}, as a function of duty-cycle and for different pitches of the SWG at $\lambda = 1.55\,\mu\mathrm{m}$. It is apparent that in order to minimize the excitation of ϕ_3 the duty-cycle has to be kept below $\sim 25\,\%$. This may be understood by examining Fig. 3(b), which shows the field of the input mode, ϕ_{in}, as well as the field of the third order supermode, ϕ_3, for two different duty-cycles and a pitch of $\Lambda = 271\,\mathrm{nm}$. For a $22\,\%$ duty-cycle ϕ_3 exhibits an almost perfect anti-symmetry with respect to ϕ_{in}, so that power transfer will be minimum. For a larger $50\,\%$ duty-cycle this anti-symmetry is broken and the overlap between ϕ_1 and ϕ_3 increases to about $5\,\%$. Such an amount of power indeed would suffice to significantly deteriorate the behavior of the coupler.

3.2. Minimizing the wavelength dependence of L_π

As discussed in the previous section the duty-cycle of the SWG structure has to be kept below $25\,\%$ to avoid unwanted power transfer to the third order supermode of the coupler. On the other hand, a duty-cycle significantly below $25\,\%$ yields reduced feature sizes which are difficult to realize. Thus, the main degree of freedom for the design of the SWG structure is its pitch, Λ. In order to achieve a fabricable design, minimum feature sizes should be around $\sim 60\,\mathrm{nm}$, which is close to the limit of most e-beam processes. This sets a lower limit of $\Lambda \geq 240\,\mathrm{nm}$ for the pitch that can be used for a realistic design of the SWG region. The upper limit of the pitch is set by the Bragg condition, which is most critical for the shortest operation wavelength. In this case we chose $\lambda_{\mathrm{min}} = 1500\,\mathrm{nm}$, so that $\Lambda \leq \lambda_{\mathrm{min}}/(2n_{\mathrm{eff}}) \approx 300\,\mathrm{nm}$, where an approximate value $n_{\mathrm{eff}} \approx 2.5$ has been assumed. We then numerically calculate L_π from the propagation constants of the two lowest order Floquet modes of the coupling region (ϕ_1 and ϕ_2). Figure 4(a) shows $L_\pi/2$ in the $1500\,\mathrm{nm}$ to $1600\,\mathrm{nm}$ wavelength range for three different pitches and a constant duty-cycle of $22.5\,\%$. For the lowest pitch, $\Lambda = 261\,\mathrm{nm}$, the behavior is similar to a conventional directional coupler [see Fig. 1(b)], with L_π increasing almost linearly as wavelength is decreased. However, as the pitch is increased to $\Lambda = 271\,\mathrm{nm}$ the Bragg wavelength of the SWG is shifted sufficiently

#164215 - $15.00 USD Received 6 Mar 2012; revised 26 Mar 2012; accepted 27 Mar 2012; published 31 May 2012

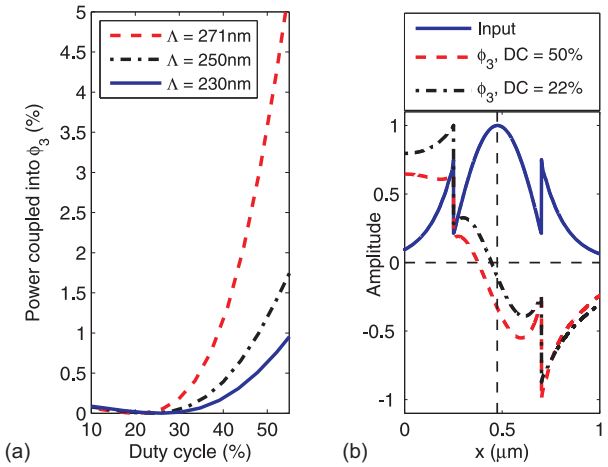

Fig. 3. (a) Power coupled from the input field, ϕ_{in}, into the third order supermode, ϕ_3, as function of duty-cycle of the SWG. (b) Field profile of the third order supermode, ϕ_3, and the input field, ϕ_{in}. Fields are shown in the lower half of the coupler.

close to actually decrease L_π for shorter wavelengths (see discussion in section 2.2). This results in a remarkable flattening of the L_π curve, which exhibits a variation of only 4 % in the 100 nm bandwidth. Thus $\Lambda = 271$ nm is chosen as the nominal pitch for our design. In fact, from Fig. 4(b) it is apparent that $n_{\text{eff},1}$ and $n_{\text{eff},2}$ no longer converge (as in the conventional coupler), but are appropriately spaced to keep L_π constant. Note that further increasing the pitch to $\Lambda =$ 281 nm results in the effect of the SWG being too strong, effectively increasing the variation of L_π [Fig. 4(a)].

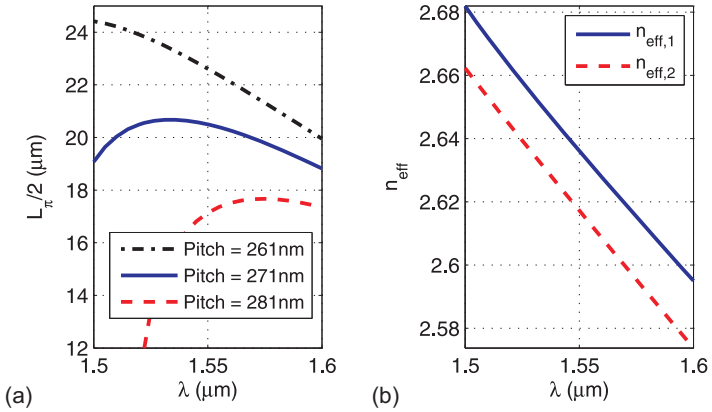

Fig. 4. (a) Half beat length ($L_\pi/2$) and (b) effective indices of the even and odd supermodes, ϕ_1 and ϕ_2, of the SWG based directional coupler as a function of wavelength for $\Lambda =$ 271 nm. Grating duty-cycle is 22.5 %.

Note that although the waveguide separation in the SWG based coupler ($s_{\text{SWG}} = 0.5\,\mu$m) is larger than in the conventional design ($s_{\text{conv}} = 0.3\mu$m), the half beat lengths of both designs are approximately equal ($L_\pi/2 \sim 20\,\mu$m). This is because for a given waveguide separation the

#164215 - $15.00 USD Received 6 Mar 2012; revised 26 Mar 2012; accepted 27 Mar 2012; published 31 May 2012

presence of the SWG reduces the beat length; in fact, removal of the SWG in the coupler in Fig. 2(a) increments the half beat length to 110 μm.

3.3. *Simulation and verification of the complete coupler*

In the final design step the complete coupler as shown in Fig. 2(a) is simulated. The separation between the access waveguides is set to $a = 1\,\mu$m to ensure they are fully decoupled, and the adiabatic s-bends are 5 μm long. The number of SWG periods, P, was optimized by 2D simulations with our in-house tool [19] to produce symmetric 50/50 coupling, yielding $P = 71$. The resulting coupling length of $P \times \Lambda = 19.2\,\mu$m is in excellent agreement with the half beat length for $\Lambda = 271$ nm shown in Fig. 4, confirming that coupling in the s-bend regions is indeed negligible. Note that other splitting ratios are readily obtained by adjusting P.

Figure 5(a) shows the output power for the bar and cross ports of the SWG based coupler. As expected from the nearly constant L_π value, output power is virtually flat in a 100 nm bandwidth. The residual ripple in the output power is attributed to small back-reflections at the ends of the SWG region. These reflections could be further reduced by tapering the SWG in the input and output regions, which, however, requires carefully studying the excitation of the third order mode. The output power of a conventional directional coupler with the same coupling length of 19.2 μm is shown for comparison in Fig. 5(a). The SWG coupler maintains an imbalance of 0.6 dB between its outputs over a 96 nm bandwidth, while the conventional coupler covers less than 20 nm of bandwidth with this imbalance. A fivefold improvement in operation bandwidth can thus be achieved with the proposed design. Figure 5(b) shows the phase shift between the outputs of the SWG based coupler, which exhibits a deviation of less than $\pm 4^\circ$ from its nominal 90° value. Back-reflections from the coupler are below -15 dB for the full operational bandwidth [Fig. 5(c)]. Note that while the device's bandwidth could be slightly enhanced in terms of imbalance by shifting the response to longer wavelengths [Fig. 5(a)], this would also increase return losses for shorter wavelengths [Fig. 5(c)].

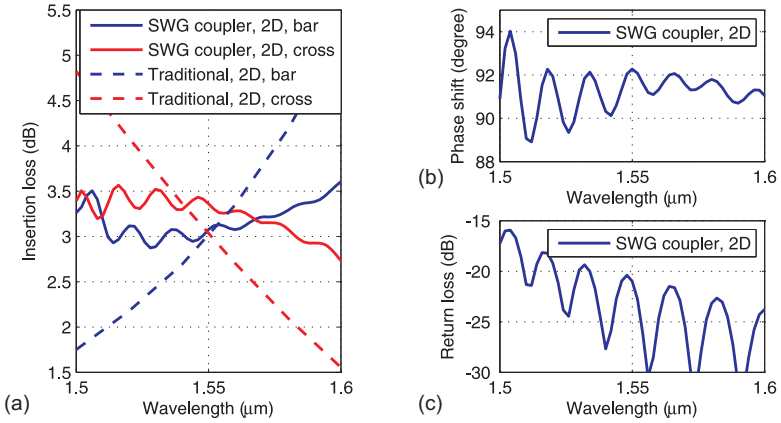

Fig. 5. (a) 2D simulation results of the output power of the proposed SWG based coupler compared to a conventional directional coupler. (b) Phase shift between the outputs of the SWG based coupler. (c) Back-reflections from the SWG based coupler.

To further validate the performance of the device full 3D FDTD simulations were carried out. We used a grid in the $x-y-z$ directions of 30 nm – 40 nm – 5 nm and a time step below the Courant limit. Despite the 2D, effective index approximation used in the above analysis, we found the predicted device dimensions to be very close to the dimensions that yield opti-

#164215 - $15.00 USD Received 6 Mar 2012; revised 26 Mar 2012; accepted 27 Mar 2012; published 31 May 2012

mum performance in the 3D case. The pitch increased by less than 1% to $\Lambda_{3D} = 273\,\text{nm}$, and the number of periods was adjusted to $P_{3D} = 84$, corresponding to a $3.5\mu\text{m}$ increase in coupling length. Some discrepancy between the 3D and 2D simulations is expected, since precise calculations of coupling lengths are challenging in 2D approximations [20]. The output power obtained with these parameters is shown in Fig. 6. While the residual ripple is less apparent in the 3D simulations, the results are in excellent agreement with the 2D modeling, thereby confirming the broadband behavior of the coupler.

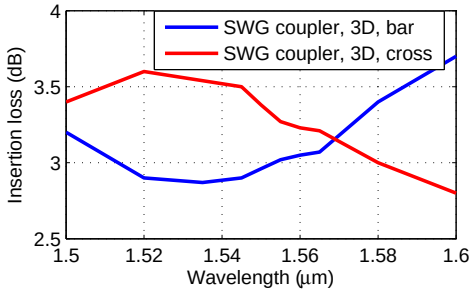

Fig. 6. 3D simulation results of the output power of the proposed SWG based coupler.

Although not within the scope of this paper, it is noted that analyzing the 3D device with a full vectorial Floquet mode solver could significantly reduce simulation times compared to 3D FDTD, and allow for further device optimization.

4. Conclusions

By exploiting the dispersive properties of sub-wavelength gratings for the first time, we have designed a directional coupler that exhibits a fivefold bandwidth enhancement compared to conventional directional couplers. Our approach yields a compact device, and does not deteriorate the coupler's phase response. The design is carried out using efficient 2D Floquet mode analysis, and validated with full 3D FDTD simulations. The concept of SWG dispersion engineering that we introduce here opens excellent prospects for dispersion management in photonic integrated devices.

Acknowledgments

This work was supported by the the Spanish Ministerio de Ciencia (project TEC2009-10152), the Andalusian Regional Ministry of Science, Innovation and Business (project P07-TIC-02946), and the European Mirthe project (FP7-2010-257980).

#164215 - $15.00 USD Received 6 Mar 2012; revised 26 Mar 2012; accepted 27 Mar 2012; published 31 May 2012